Proceedings of the Sixteenth International Conference on Computational Structures Technology
Edited by: P. Iványi, J. Kruis and B.H.V. Topping
Civil-Comp Conferences, Volume 14, Paper 14.1
Civil-Comp Press, Edinburgh, United Kingdom, 2026
ISSN: 2753-3239, doi: 10.4203/ccc.14.14.1
©Civil-Comp Ltd, Edinburgh, UK, 2026

Limit Analysis for Pagoda of Zhen-Guo Temple: Comparison of Different Modeling Approaches

P. Wang[1], Y. Hua[2] and G. Milani[2]

[1]Yangzhou University, China

[2]Politecnico di Milano, Italy

Abstract

Masonry pagodas constitute a large proportion of Chinese architectural heritage. Despite standing for hundreds of years, these structures have accumulated various forms of damage, making them increasingly vulnerable to natural hazards and extreme loads. Furthermore, their characteristic slenderness significantly compromises their seismic resistance. This paper aims to explore a suitable modeling approach for masonry pagodas within the limit analysis framework, providing a rapid tool that could serve in the further seismic vulnerability analysis of these constructions. In recent numerical studies based on 3D limit analysis, the deformability of the masonry is usually not fully taken into account, and the material plasticity is typically reduced to the interfaces. This contribution develops formulations for 3D limit analysis that allow both element dissipation and interfacial discontinuity, which can eventually be formulated as standard Second-Order Cone Programming (SOCP). Implementing the formulations, the collapse of the pagoda in Zhen-Guo Temple is investigated as a case study. Three different models for the pagoda are compared, considering either element dissipation or interfacial discontinuities. The results are also benchmarked with the previous finite element solution for validation. The comparative studies have highlighted that accounting for energy dissipation at both elements and interfaces is essential when simulating the collapse of masonry pagodas. However, the suitability of the constitutive model for interfaces and elements remains an ongoing investigation, which is essential for precisely reproducing the typical crack propagation in pagoda collapses.

Keywords: 3D limit analysis, masonry pagoda, second-order cone programming, homogeneous modeling, rigid block modeling, seismic loading.

1 Introduction

Chinese masonry pagodas originated from the integration of local architectural traditions following the introduction of Buddhism during the Eastern Han Dynasty. As the most numerous and widely distributed type of ancient architecture in China, they embody the historical memory and cultural heritage of Chinese civilization. These pagodas serve not only as carriers of religious beliefs but also as comprehensive manifestations of ancient construction techniques, artistic aesthetics, and engineering wisdom. Ancient masonry structures in China typically employed low-strength lime mortar, resulting in poor overall shear performance [1] and thereby high vulnerability to seismic loads. Moreover, millennia of material aging have significantly degraded the structural performance of these pagodas [2]. Therefore, a reliable assessment of their residual capacity is essential for the scientific conservation of these historic structures.

Common simulation techniques for masonry structures rely on Finite Element Analysis (FEA), which has been supported by several commercial software packages [3]. This approach is also applicable to masonry pagodas [4], providing detailed information on stress distribution, material softening, and brittle failure mechanisms at the post-peak stage. The material behavior of masonry is typically described using the Concrete Damaged Plasticity (CDP) model, in which damage indices implicitly capture crack propagation during structural failure. However, the CDP model requires a couple of material parameters that are difficult to obtain, and its high computational cost further limits its application in vulnerability analyses.

In contrast, limit analysis has long been a classical approach to evaluating the failure of masonry systems. It requires a few material parameters and relatively low computational cost, while naturally accounting for interfacial discontinuities. In the last century, this approach was developed into a modern numerical technique based on several pioneering contributions [5–8]. Over recent decades, its application to masonry structures has often employed rigid block modeling to accurately represent the actual bond pattern (e.g., [9-11]). However, for larger constructions such as pagodas, a precise representation of heterogeneity is virtually impractical, as it would require, on the one hand, considerable computational expense, and on the other hand, high-precision field surveys. Therefore, suitable homogenization techniques are necessary to be adopted. Nevertheless, in recent full 3D applications of masonry homogenization, the deformability of the elements is typically precluded [12-14], which may introduce inaccuracies, particularly when using a well-aligned structured mesh.

In this paper, we will present a 3D limit analysis for a Chinese masonry pagoda structure with application of different modeling strategies, including a) rigid elements with interfaces, b) deformable elements without interfaces, and c) deformable elements with interfaces. These problems can all be solved using a reliable Second-Order Cone Programming (SOCP) algorithm with an acceptable computational burden. Section 2 will elucidate the establishment of these 3D limit analysis formulations. The element and interfacial plasticity will be described using the 3D Drucker-Prager criterion and 3D Mohr-Coulomb friction, respectively. Section 3 presents a collapse analysis of the pagoda at Zhen-Guo Temple under uniaxial seismic loading to evaluate the performance of the different modeling approaches proposed. This case study has been previously analyzed using an FEA approach in [15]. We will also compare our results to this reference to demonstrate the fidelity of the limit-analysis-based solution. Major conclusions will be drawn in Section 4.

2 Methodology

This section briefly revisits the development of 3D upper-bound limit analysis using deformable discretization with interfacial discontinuities proposed in [16]. Combined with the associated flow rule, the collapse problem is formulated as a standard Second-Order Cone Programming (SOCP) problem amenable to robust solution algorithms. This formulation can be plainly reduced to the case for continuous deformable meshes or rigid blocks with interfaces, thereby enabling the three distinct models for the masonry pagoda.

2.1 Compatibility condition

When the constant-strain field is adopted to describe the element deformability, its velocity distribution is completely determined by 12 components: 6 for rigid-body motion and 6 for the constant-strain mode (collected in $\mathbf{u}_{\mathrm{P}}^{i}$ in Eq. (1)). These components can then be mapped to construct the velocity field of the element by matrix $\mathbf{H}_{\mathrm{P}}(\mathbf{r})$ (Eq. (2)), whose columns form the bases of the rigid-body space and constant-strain space (Eq. (3)).

$$
\begin{aligned}
\mathbf{u}_{\mathrm{P}}^{i} &= \begin{bmatrix} \mathbf{u}_{\mathrm{R}}^{i} & \mathbf{u}_{\mathrm{C}}^{i} \end{bmatrix}^{T} \\
\mathbf{u}_{\mathrm{R}}^{i} &= \begin{bmatrix} u_{x}^{i} & u_{y}^{i} & u_{z}^{i} & \omega_{xy}^{i} & \omega_{yz}^{i} & \omega_{zx}^{i} \end{bmatrix} \\
\mathbf{u}_{\mathrm{C}}^{i} &= \begin{bmatrix} \varepsilon_{x}^{i} & \varepsilon_{y}^{i} & \varepsilon_{z}^{i} & \varepsilon_{xy}^{i} & \varepsilon_{yz}^{i} & \varepsilon_{zx}^{i} \end{bmatrix}
\end{aligned}
\tag{1}
$$

$$
\mathbf{u}^{i}(\mathbf{r}) = \mathbf{H}_{\mathrm{P}}(\mathbf{r})\mathbf{u}_{\mathrm{P}}^{i}, \ \mathbf{r} := \begin{bmatrix} x-\bar{x} & y-\bar{y} & z-\bar{z} \end{bmatrix}^{T}
\tag{2}
$$

$$
\mathbf{H}_{\mathrm{P}}(\mathbf{r}) = \left[\begin{array}{cccccc|cccccc}
1 & & & -\mathbf{r}_{(2)} & & \mathbf{r}_{(3)} & \mathbf{r}_{(1)} & & & \mathbf{r}_{(2)} & & \mathbf{r}_{(3)} \\
 & 1 & & \mathbf{r}_{(1)} & -\mathbf{r}_{(3)} & & & \mathbf{r}_{(2)} & & \mathbf{r}_{(1)} & \mathbf{r}_{(3)} & \\
 & & 1 & & \mathbf{r}_{(2)} & -\mathbf{r}_{(1)} & & & \mathbf{r}_{(3)} & & \mathbf{r}_{(2)} & \mathbf{r}_{(1)}
\end{array}\right]
\tag{3}
$$

$$
\begin{aligned}
\mathbf{q}_{j} &= \begin{bmatrix} \Delta u_{n,1}^{j}, \Delta u_{s,1}^{j}, \Delta u_{t,1}^{j}, \cdots, \Delta u_{n,k}^{j}, \Delta u_{s,k}^{j}, \Delta u_{t,k}^{j} \end{bmatrix}^{T} \\
&= \begin{bmatrix} -\left(\mathbf{A}_{j,\mathrm{P}}^{a}\right)^{T} & \left(\mathbf{A}_{j,\mathrm{P}}^{b}\right)^{T} \end{bmatrix} \begin{bmatrix} \mathbf{u}_{\mathrm{P}}^{a} \\ \mathbf{u}_{\mathrm{P}}^{b} \end{bmatrix}
\end{aligned}
\tag{4}
$$

Regarding the interface kinematics, each node of the interface is assigned one normal and two tangential degrees of freedom to describe the nodal discontinuities, all of which are checked to follow the plasticity flow rule. These discontinuities can be computed by subtracting the velocities at overlapped nodes and then projecting onto the local coordinate system. Nodal velocities are associated with the relevant element unknowns (see Eq. (2)). Finally, the velocity jumps at each interface $\mathbf{q}_j$ can be expressed in terms of the element unknowns of the two associated blocks (Eq. (4)), connected by the compatibility matrix $\mathbf{A}_{j,\mathrm{P}}^{i}$ (Eq. (4)). The global matrix form of this condition can be written as Eq. (6).

$$\begin{aligned}
&\mathbf{A}_{j,\mathrm{P}}^{i}=\begin{bmatrix}\mathbf{Q}_j\mathbf{H}_{\mathrm{P}}^{i}\left(\mathbf{r}_1^{i}\right)\\ \vdots\\ \mathbf{Q}_j\mathbf{H}_{\mathrm{P}}^{i}\left(\mathbf{r}_k^{i}\right)\end{bmatrix}^T,\ i=a,b,\ k=V\left(\mathrm{F}_j^{a}\cap\mathrm{F}_j^{b}\right)\\
&\mathbf{Q}_j=\begin{bmatrix}\mathbf{e}_{\mathrm{n}}^{j} & \mathbf{e}_{\mathrm{s}}^{j} & \mathbf{e}_{\mathrm{t}}^{j}\end{bmatrix}^T
\end{aligned}\tag{5}$$

$$\mathbf{A}^T\mathbf{u}_{\mathrm{P}}=\mathbf{q}\tag{6}$$

2.2 Interfacial constitutive model and associated flow rule

The interfacial constitutive model adopts the Mohr-Coulomb friction theory [17]. For 3D cases, the tangential force resultant $\left\|\left(x_{s,k}^{j},x_{t,k}^{j}\right)\right\|_2$ at each node pair is bounded by the normal force $-\mu x_{n,k}^{j}$ and additional cohesion $c_0\overline{A}_k^{j}$ (see Eq. (7)). The corresponding yield surface is a second-order cone.

$$\forall j,k,\ -\mu x_{n,k}^{j}+c_0\overline{A}_k^{j}\le\left\|\left(x_{s,k}^{j},x_{t,k}^{j}\right)\right\|_2\tag{7}$$

The matrix form of the constitutive relation can be expressed as Eq. (8) by introducing the slackness variables $\mathbf{z}_0$. Equivalently, the slack variables of all nodal pairs must belong to the standard 3D second-order cone Q^3. Eq. (9) lists the components of the constitutive operator $\mathbf{N}$ and cohesion vector $\mathbf{c}_0$ for node pair k on interface j.

$$\mathbf{N}\mathbf{x}-\mathbf{c}_0=-\mathbf{z}_0,\ \mathbf{z}_0\in\mathrm{Q}_1^3\times\mathrm{Q}_2^3\times\cdots\times\mathrm{Q}_l^3\tag{8}$$

$$\mathbf{N}_{j,k}=\mathrm{diag}\left(\begin{bmatrix}\tan\varphi & 1 & 1\end{bmatrix}\right),\ \mathbf{c}_{0,k}^{j}=\begin{bmatrix}c_0\overline{A}_k^{j} & 0 & 0\end{bmatrix}^T\tag{9}$$

For interfaces where the nodal resultant reaches the yield surface, the flow direction is assumed to be perpendicular to the yield tangent plane (i.e., associated flow rule), which can be represented by a conic constraint dual to the constitutive one. In terms of the matrix representation, the introduced plastic multipliers $\mathbf{p}$ must lie in the standard quadratic cone, and these multipliers will be associated with the interfacial velocity jumps $\mathbf{q}$ (see Eq. (10)). Dissipation power is the inner product of total interfacial resultants and velocity jumps, which can be written as a linear expression of plastic multiplier $\mathbf{p}$ (Eq. (11)).

$$\mathbf{A}^T\mathbf{u}_{\mathrm{P}}=\mathbf{q}=\mathbf{N}^T\mathbf{p},\ \mathbf{p}\in\mathrm{Q}_1^3\times\mathrm{Q}_2^3\times\cdots\times\mathrm{Q}_l^3\tag{10}$$

$$P_D^{\mathrm{C}}=\mathbf{c}_0^T\mathbf{p}\tag{11}$$

2.3 Element constitutive model and associated flow rule

At the element level, the classical 3D Mohr-Coulomb (MC) model produces a semi-definite constraint rather than a quadratic cone constraint [18]. Solving Semi-Definite Programming (SDP) is more time-consuming and less robust than solving SOCP. The 3D Drucker-Prager (DP) criterion is therefore adopted as the constitutive model of the dissipative elements, which is a quadratic conic approximation of the MC pyramid surface [19].

$$f\left(I_1, J_2\right) = aI_1 + \sqrt{J_2} - k \le 0 \tag{12}$$

$$a = \frac{2\sin\varphi}{\sqrt{3}\left(3-\sin\varphi\right)},\ k = \frac{6c\cos\varphi}{\sqrt{3}\left(3-\sin\varphi\right)} \tag{13}$$

The standard DP constraint (Eq. (12)) involves stress invariants I_1 and J_2. To maintain consistency with the FEA simulation in [15], the DP-II approximation is employed, whose yield surface circumscribes the actual MC one. Eq. (13) provides the corresponding coefficients α and k, which can be calculated from cohesive and frictional properties of the material. Expressing in matrix form, the slackness variable $\mathbf{z}_1$ should lie inside the standard 7-dimensional quadratic cone (Eq. (14)).

$$\begin{gathered}\mathbf{M}\tilde{\boldsymbol{\sigma}} - \mathbf{c}_1 = -\mathbf{z}_1,\ \mathbf{z}_1 \in \mathrm{Q}_1^7 \times \mathrm{Q}_2^7 \times \cdots \times \mathrm{Q}_{N_e}^7 \\ \tilde{\boldsymbol{\sigma}}_i := \left|E_i\right| \begin{bmatrix} \sigma_x^i & \sigma_y^i & \sigma_z^i & 2\tau_{xy}^i & 2\tau_{yz}^i & 2\tau_{zx}^i \end{bmatrix}^T\end{gathered} \tag{14}$$

Element plastic flow is represented by a reciprocal conic constraint (Eq. (15)), due to assuming the associated flow rule. The deformation components are linked to the multipliers by the matrix $\mathbf{M}^T$. On the left-hand side of Eq. (15), matrix $\mathbf{B}$ extracts strain rates from the global unknown list. The block matrix $\mathbf{B}_i$ for element i is assembled by combining zero matrices and identity matrices.

$$\mathbf{B}^T\mathbf{u}_{\mathrm{P}} = \mathbf{u}_{\mathrm{C}} = \mathbf{M}^T\boldsymbol{\lambda},\ \boldsymbol{\lambda} \in \mathrm{Q}_1^7 \times \mathrm{Q}_2^7 \times \cdots \times \mathrm{Q}_e^7,\ \mathbf{B}_i := \begin{bmatrix} \mathbf{O}_{6\times6} & \mathbf{I}_{6\times6} \end{bmatrix}^T \tag{15}$$

$$P_D^{\mathrm{E}} = \mathbf{c}_1^T\boldsymbol{\lambda} \tag{16}$$

Elemental dissipation is proportional to plastic multipliers and correlates with element cohesion (Eq. (16)), featuring a similar form with interfacial dissipation (Eq. (11)).

2.4 Limit analysis formulation for different modeling

Eventually, the Upper bound (UB) limit analysis of 3D deformable elements can be formulated as Eq. (17), incorporating the additional normalized positive work condition [20]. We minimize the total dissipation and external power subject to compatibility and flow-rule constraints. Vector $\mathbf{f}_D$ and $\mathbf{f}_L$ contain the dead and live load information. The optimization has a similar form to the 2D case [21-22], except that plastic multipliers are confined to the quadratic cones instead of being non-negative.

According to duality theory, we derive the static form of Upper Bound limit analysis (Eq. (18)), which is also an SOCP problem. This formulation considers the equilibrium condition and constitutive constraints for elements and interfaces to maximize the collapse multiplier, consistent with the 2D formulation as well.

$$\begin{aligned}
\text{min.}\quad & -\mathbf{f}_D^T\mathbf{u}_\mathrm{P}+\mathbf{c}_0^T\mathbf{p}+\mathbf{c}_1^T\boldsymbol{\lambda}\\
\text{s.t.}\quad & \mathbf{f}_L^T\mathbf{u}_\mathrm{P}=1\\
& \mathbf{A}^T\mathbf{u}_\mathrm{P}=\mathbf{N}^T\mathbf{p},\ \mathbf{p}\in \mathrm{Q}_1^3\times\mathrm{Q}_2^3\times\cdots\times\mathrm{Q}_l^3\\
& \mathbf{B}^T\mathbf{u}_\mathrm{P}=\mathbf{M}^T\boldsymbol{\lambda},\ \boldsymbol{\lambda}\in \mathrm{Q}_1^7\times\mathrm{Q}_2^7\times\cdots\times\mathrm{Q}_e^7
\end{aligned}\tag{17}$$

$$\begin{aligned}
\text{max.}\quad & \alpha\\
\text{s.t.}\quad & \mathbf{A}\mathbf{x}+\mathbf{B}\tilde{\boldsymbol{\sigma}}=\alpha\mathbf{f}_L+\mathbf{f}_D\\
& \mathbf{c}_0-\mathbf{N}\mathbf{x}\in \mathrm{Q}_1^3\times\mathrm{Q}_2^3\times\cdots\times\mathrm{Q}_l^3\\
& \mathbf{c}_1-\mathbf{M}\tilde{\boldsymbol{\sigma}}_1\in \mathrm{Q}_1^7\times\mathrm{Q}_2^7\times\cdots\times\mathrm{Q}_e^7
\end{aligned}\tag{18}$$

As we have claimed, Eqs. (17) and (18) can be straightforwardly degraded to two specific cases that preclude the element or interfacial dissipation. When the element is not deformable, the element compatibility and flow rule can be removed. The corresponding constitutive constraint for the element plasticity can also be wiped out on the static side. The formulation thereby becomes exactly the classical 3D rigid block limit analysis (Eqs. (19) and (20)).

$$\begin{aligned}
\text{min.}\quad & -\mathbf{f}_D^T\mathbf{u}_\mathrm{R}+\mathbf{c}_0^T\mathbf{p}\\
\text{s.t.}\quad & \mathbf{f}_L^T\mathbf{u}_\mathrm{R}=1\\
& \mathbf{A}^T\mathbf{u}_\mathrm{R}=\mathbf{N}^T\mathbf{p},\ \mathbf{p}\in \mathrm{Q}_1^3\times\mathrm{Q}_2^3\times\cdots\times\mathrm{Q}_l^3
\end{aligned}\tag{19}$$

$$\begin{aligned}
\text{max}\quad & \alpha\\
\text{s.t.}\quad & \mathbf{A}\mathbf{x}+\mathbf{B}\tilde{\boldsymbol{\sigma}}=\alpha\mathbf{f}_L+\mathbf{f}_D\\
& \mathbf{c}_0-\mathbf{N}\mathbf{x}\in \mathrm{Q}_1^3\times\mathrm{Q}_2^3\times\cdots\times\mathrm{Q}_l^3
\end{aligned}\tag{20}$$

$$\begin{aligned}
\text{min.}\quad & -\mathbf{f}_D^T\mathbf{u}_\mathrm{P}+\mathbf{c}_1^T\boldsymbol{\lambda}\\
\text{s.t.}\quad & \mathbf{f}_L^T\mathbf{u}_\mathrm{P}=1\\
& \mathbf{A}^T\mathbf{u}_\mathrm{P}=\mathbf{0}\\
& \mathbf{B}^T\mathbf{u}_\mathrm{P}=\mathbf{M}^T\boldsymbol{\lambda},\ \boldsymbol{\lambda}\in \mathrm{Q}_1^7\times\mathrm{Q}_2^7\times\cdots\times\mathrm{Q}_e^7
\end{aligned}\tag{21}$$

$$\begin{aligned}
\text{max.}\quad & \alpha\\
\text{s.t.}\quad & \mathbf{A}\mathbf{x}+\mathbf{B}\tilde{\boldsymbol{\sigma}}=\alpha\mathbf{f}_L+\mathbf{f}_D\\
& \mathbf{c}_1-\mathbf{M}\tilde{\boldsymbol{\sigma}}_1\in \mathrm{Q}_1^7\times\mathrm{Q}_2^7\times\cdots\times\mathrm{Q}_e^7
\end{aligned}\tag{22}$$

We can also cancel the interfacial discontinuities to formulate the continuous finite element limit analysis (Eqs. (21) and (22)) by simply enforcing the interfacial plasticity multiplier **p** equal to zero. In the static formulation, the second interfacial constitutive constraint is no longer required as the interfacial force can be arbitrary if the overlapped nodes are perfectly coupled.

3 Results

By implementing the proposed formulations, the three aforementioned models for masonry pagodas can be constructed. In this section, the pagoda of Zhen-Guo Temple in China will be taken as an example. The structural analysis of this pagoda has been previously carried out using FEA software in [15]. Therefore, on top of presenting the limit analysis solutions, these results will also be compared with the FEA reference solutions to validate the reliability of the proposed limit analysis modeling in the collapse simulation of the masonry pagoda.

3.1 Case study: Pagoda of Zhen-Guo Temple

The Zhen-Guo Temple Pagoda, first built in the Tang Dynasty (874-888 AD), is located on an island in Gaoyou, Jiangsu Province, China. It is a square seven-story pavilion-style brick pagoda with a total height of 35.36 meters (Fig. 1a). Having undergone multiple repairs, the existing structure integrates architectural styles from the Tang, Song, and Ming dynasties. In 2014, the pagoda was inscribed as part of the Beijing-Hangzhou Canal on the World Heritage List. The pagoda has a square plan, with both side lengths and wall thicknesses gradually decreasing from bottom to top. Its interior features timber floors and timber stairs. The pagoda's exterior retains the masonry style of the Tang Dynasty, while the dougong and eaves exhibit characteristics of the Ming Dynasty.

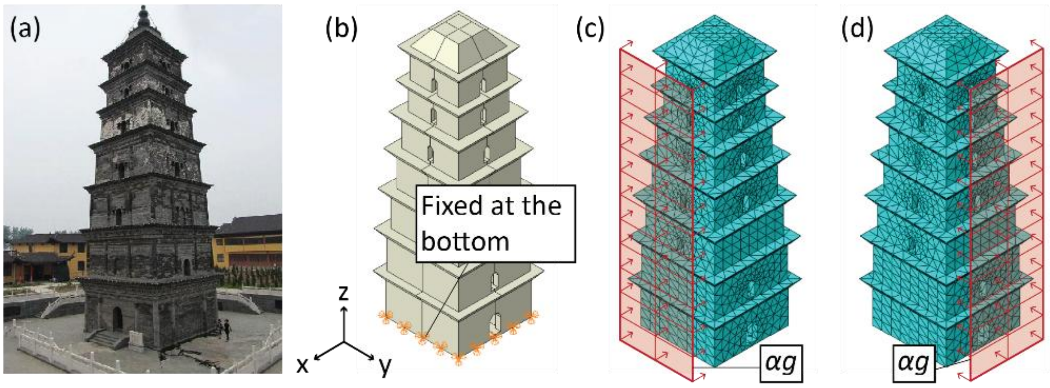

Fig. 1. Pagoda of Zhen-Guo Temple: a) on-site photo; b) geometry model and boundary conditions; c) X direction loading; c) Y direction loading.

According to the on-site survey, the geometry of the pagoda is modelled using CAD software. This model is then imported into ABAQUS for discretization (Fig. 1b), and the total number of tetrahedra is about 18500. An interface has been implemented in MATLAB to read mesh information from the INP file, a standard exchange file format of the ABAQUS software. Further calculations of the limit analysis are completed in MATLAB. The constructed SOCP problem is solved through the MOSEK code package. Corresponding to the three limit analysis formulations proposed, three modeling strategies for the pagoda are considered: a) rigid elements with interfaces; b) deformable elements without interfaces; c) deformable elements with interfaces.

Given that employing a homogeneous consideration of masonry bond patterns, the material properties of the elements and interfaces should be derived from a suitable homogenization. According to the on-site investigation, the strength of the brick and mortar is around 15-20MPa and 1.5-2.5MPa [15]. We therefore assign the masonry cohesion equal to the shear strength suggested in the Chinese masonry code [23]. The friction coefficient is assumed to be 0.65, which is the average of the friction coefficients for dry and moist interfacial conditions [23]. The material density is consistent with that used in FEA simulation [15]. All the parameters used have been listed in Table 1.

Table 1. Material properties of the Pagoda

Cohesion c_m [MPa]	Friction angle φ_m [°]	Density ρ [kg/m^3]
0.13	33	2000

A seismic loading scenario has been considered in this analysis, which, in the context of limit analysis, is simplified as a horizontal pushover. We take into account both loading directions in X and Y, and the imposed acceleration distribution is uniform along the height of the pagoda (see Fig. 1c and 1d). The boundary condition at the bottom of the pagoda follows the setting in the FEA simulation [15], where the nodal degrees of freedom are all fixed in three directions.

3.2 Collapse results predicted from different modeling approaches

Fig. 2 displays the collapse of the pagoda predicted from rigid tetrahedral elements with dissipative interfaces. Due to geometrical symmetry, the collapse mechanism under seismic loading in both the X and Y directions is typically consistent, resulting in similar predictions for the collapse load. We can observe a significant long vertical crack in the middle of the pagoda, arising from the first floor to the top. Horizontal and sloped cracks developed at approximately the first-floor level on the rear and front facades (relative to the seismic direction), respectively, causing a noticeable tilt of the entire structure. This mechanism is quite compatible with one typical collapse of the masonry tower reported in [24] (type 4). Nevertheless, the collapse loads predicted are both higher than those obtained from the pushover analysis in [15], with an overestimation of about 65%.

The inclusion of dissipation in the elements decreases the resistance of the pagoda when it collapses (Fig. 3), although the prediction remains 45% higher than the FEA solutions. Due to the preclusion of interfacial discontinuities, the main cracks observed in the rigid element modeling cannot be realized, but are equivalently demonstrated by the dissipation in the elements. At the bottom of the pagoda, we can notice a high-dissipative area, whose location is compatible with the bottom two cracks in the rigid case (see Fig. 2). In this case, the behavior of the pagoda is more likely a cantilever beam subject to bending. The dissipative region observed at the base of the pagoda is likely attributable to the compression or tension failure of the material. At the front, the bending compression also causes a slight horizontal dilation at the bottom.

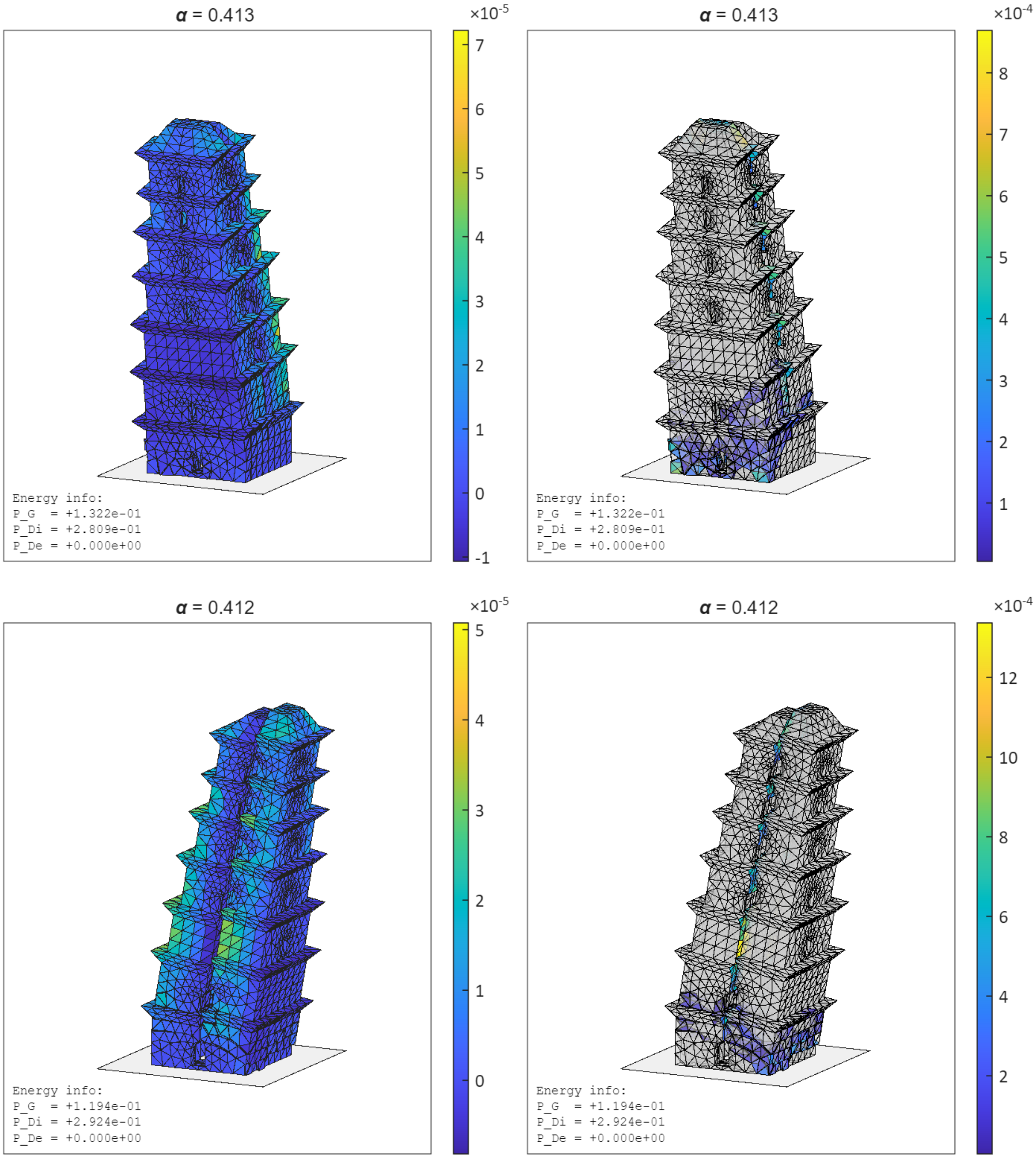

Fig. 2. Collapse of Pagoda of Zheng Guo Temple, rigid modeling with interfaces. X-direction seismic loading: top-left, gravity power; top-right, interfacial dissipation. Y-direction seismic loading: bottom-left, gravity power; bottom-right, interfacial dissipation.

Additional activation of the interface further decreases the collapse load of the pagoda (Fig. 4), which is now comparable to the FEA prediction (within 9%). In this case, the bottom two cracks are shared by the deformation of the surrounding elements, whereas the long vertical cracks are reproduced to some extent. This explains the further decrease in the structural resistance when using this modeling approach. The presence of interfacial separations releases the element dissipation. Therefore, the total dissipation of the system is much lower than that using the continuous mesh.

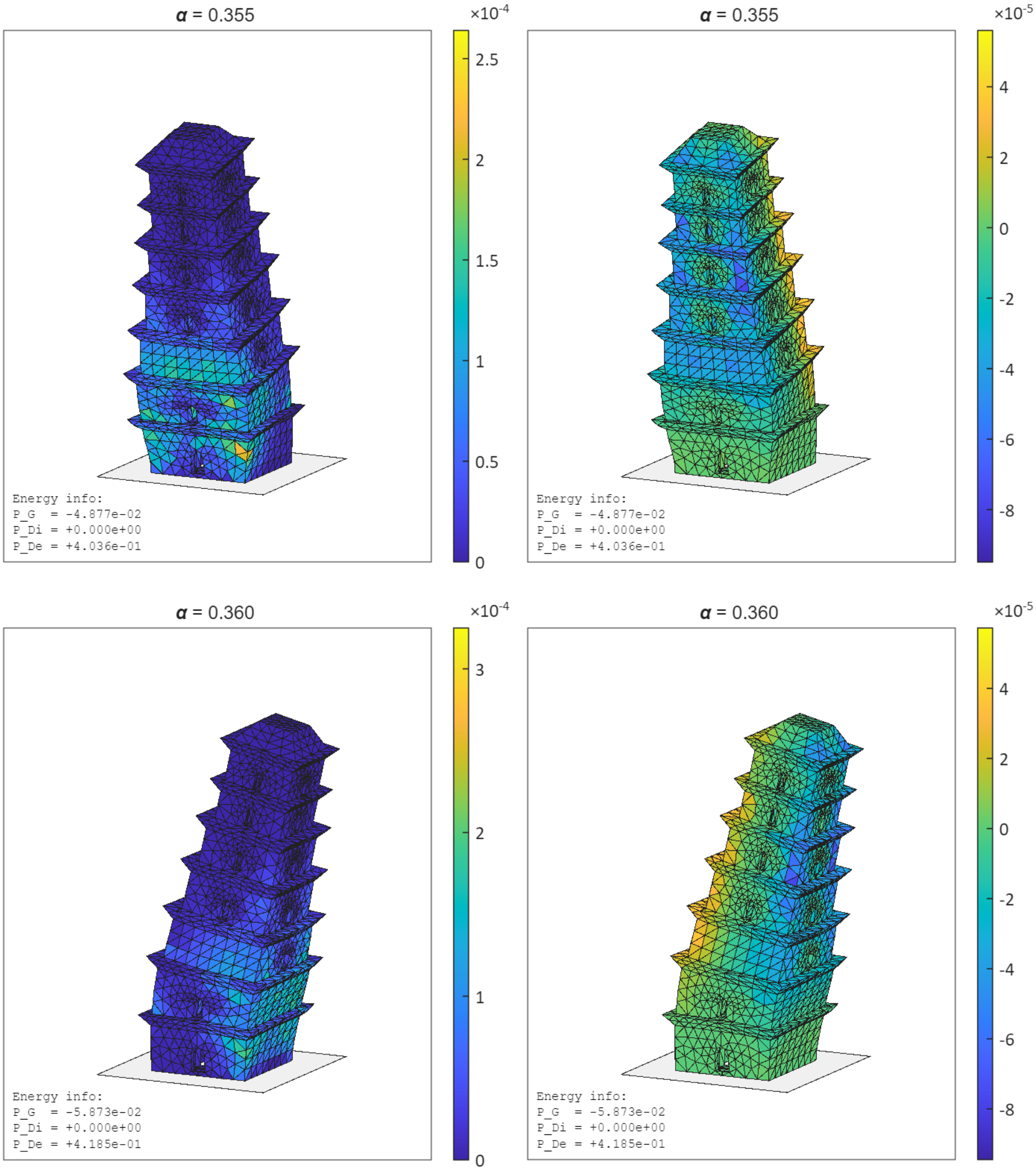

Fig. 3. Collapse of Pagoda of Zheng Guo Temple, deformable modeling without interfaces. X-direction seismic loading: top-left, element dissipation; top-right, gravity power. Y-direction seismic loading: bottom-left, element dissipation; bottom-right, gravity power.

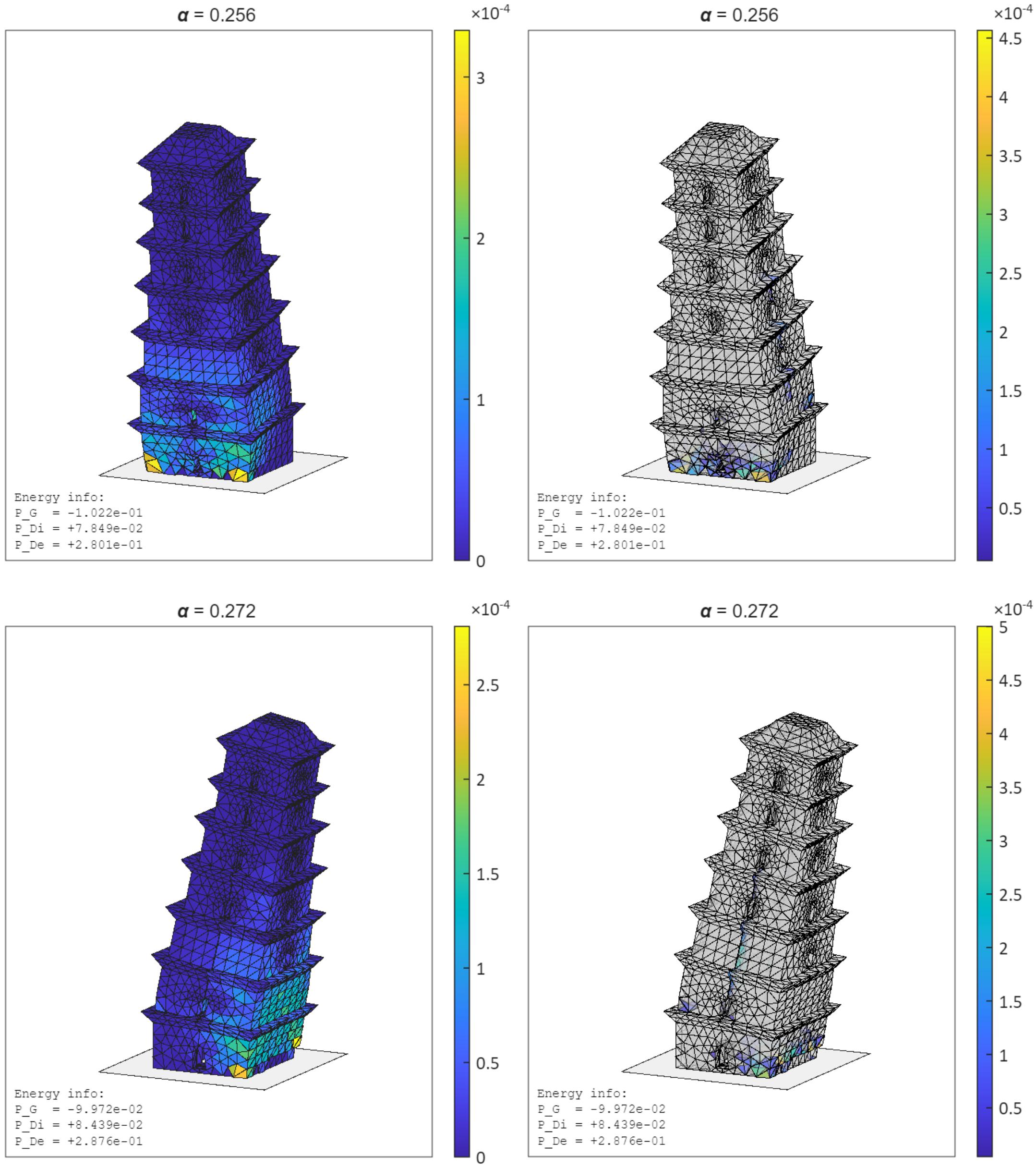

Fig. 4. Collapse of Pagoda of Zheng Guo Temple, deformable modeling with interfaces. X-direction seismic loading: top-left, element dissipation; top-right, interfacial dissipation. Y-direction seismic loading: bottom-left, element dissipation; bottom-right, interfacial dissipation.

Table 2 provides a comparison of the predicted collapse loads and the associated time costs for all the limit analysis models evaluated. According to the current case study, the inclusion of the element and interfacial dissipation is critical to warrant the accuracy of the prediction. However, the computational time required by this model will be approximately twice that of the classical rigid block limit analysis implementation. At the end of the day, these computational budgets seem quite acceptable for the problem scale of this pagoda.

Table 2. Summary of the results and corresponding time costs

Loading case	Modeling approach		Collapse acceleration [g]	Time cost [s]	FEM reference results [g]
	Deformability	Interfaces			
X direction	No	Yes	0.413	16.189	0.25
	Yes	No	0.355	33.269	
	Yes	Yes	0.256	38.213	
Y direction	No	Yes	0.412	14.707	0.25
	Yes	No	0.360	36.579	
	Yes	Yes	0.272	32.451	

4 Conclusions

This paper has proposed several limit analysis models for the masonry pagoda in Zhen-Guo Temple to evaluate the influence of element and interfacial dissipation on its collapse behavior. The constitutive models for the interfaces and elements are 3D Mohr-Coulomb friction and 3D Drucker-Prager plasticity, respectively, and the limit analysis problems for all modeling approaches can be formulated as standard Second-Order Cone Programming (SOCP). Utilizing the proposed formulations, the collapse predictions obtained from different modeling strategies are compared. These results are then benchmarked against the finite element solutions provided in the numerical reference [15] to assess the fidelity of the proposed limit analysis models.

In terms of load prediction, the most accurate model incorporates both element deformation and interface discontinuities, compared to the previous FEA reference. However, in the mechanism, the long vertical cracks, which should be typically present in a pagoda collapse, can only be partially reproduced. The two bottom tensile cracks almost vanish and are smeared in the deformation of the surrounding elements. The time consumption of this model is acceptable, but it is twice that of using rigid elements. In contrast, the implementation of the classical 3D rigid block limit analysis can produce a fairly reasonable pagoda failure mechanism, whereas the corresponding load prediction is highly overestimated. The collapse load predicted from the continuous deformable mesh stays between. However, this model fails to account for the typical crack patterns observed in pagoda collapses, a crucial feature in understanding the failure mechanisms of such structures. Future work will focus on the calibration of material parameters to investigate their impact on the collapse behavior of the pagoda, as modeled by various approaches. We will also explore a more precise representation of the element and interfacial constitutive models, incorporating essential features such as a tension cut-off. This refinement is expected to enhance the accuracy of crack reproduction in pagoda collapses.

References

[1] J.L. Yuan, “Simplified calculation method of basic period of ancient masonry pagoda”, Earthq. Eng. Eng. Vib. 35(02), 151 – 156, 2015.

[2] J.L. Lu, J.H. Si, P.G. Tian, “Test and analysis of the dynamic characteristics of the pagoda of Xingjiao temple”, Archit. Struct. 47(21),105 – 108, 2017.

[3] A.M. D’Altri, V. Sarhosis, G. Milani, J. Rots, S. Cattari, S. Lagomarsino, E. Sacco, A. Tralli, G. Castellazzi, S. de Miranda, “Modeling Strategies for the Computational Analysis of Unreinforced Masonry Structures: Review and Classification”, Arch. Computat. Methods. Eng. 27, 1153 – 1185, 2020.

[4] A. De Iasio, P.X. Wang, J. Scacco, G. Milani, S.C. Li, “Longhu pagoda: Advanced numerical investigations for assessing performance at failure under horizontal loads”, Eng. Struct. 244(June), 112715, 2021.

[5] J. Heyman, “The safety of masonry arches. In: Masonry Bridges, Viaducts and Aqueducts”, pp 329–352, 2017.

[6] J. Heyman, “The stone skeleton”, Int. J. Solids. Struct. 2:249–256, IN1–IN4, 257–264, IN5–IN12, 265–279, 1966.

[7] A. Kooharian, “Limit Analysis of Voussoir (Segmental) and Concrete Archs”, ACI J. Proc. 49,317–328, 1952.

[8] A.J.S. Pippard, “The Approximate Estimation of Safe Loads on Masonry Bridges”, Civ. Eng. War. 1, 365-372, 1948.

[9] F. Portioli, L. Cascini, “Assessment of masonry structures subjected to foundation settlements using rigid block limit analysis”, Eng. Struct. 113, 347–361, 2016.

[10] M. Rossi, C. Calderini, B. Di Napoli, L. Cascini, F. Portioli, “Structural analysis of masonry vaulted staircases through rigid block limit analysis”, Structures 23, 180–190, 2020.

[11] R. Gagliardo, L. Cascini, F.P.A. Portioli, “3D Rigid Block Limit Analysis of a Masonry Cross Vault Subjected to Shaking Table Tests”, Int. J. Archit. Herit. 18, 1886–1899, 2024.

[12] E. Reccia, G. Milani, A. Cecchi, A. Tralli, “Full 3D homogenization approach to investigate the behavior of masonry arch bridges: The Venice trans-lagoon railway bridge”, Constr. Build. Mater. 66, 567–586, 2014.

[13] P. Wang, G. Milani, “Seismic vulnerability prediction of masonry aggregates: Iterative Finite element Upper Bound limit analysis approximating no tensile resistance”, Eng. Struct. 293, 116595, 2023.

[14] G. Milani, P.B. Lourenço, “3D non-linear behavior of masonry arch bridges”, Comput. Struct. 110–111, 133–150, 2012.

[15] P. Wang, G. Liu, S. Li, “Multidimensional Analysis of Seismic Response of Zhenguo Temple Pagoda”, Lect. Notes Civ. Eng. 746 LNCE, 818–825, 2025.

[16] Y. Hua, G. Milani, 3D upper bound limit analysis for masonry arch bridges interacting with backfill, Eng. Struct. 359, 122663, 2026.

[17] L. Cascini, R. Gagliardo, F. Portioli, "LiABlock_3D: A Software Tool for Collapse Mechanism Analysis of Historic Masonry Structures", Int. J. Archit. Herit. 14, 75–94, 2020.

[18] K. Krabbenhøft, A. V. Lyamin, S.W. Sloan, "Three-dimensional Mohr-Coulomb limit analysis using semidefinite programming", Commun. Numer. Methods Eng. 24, 1107–1119, 2008.

[19] K. Krabbenhøft, A. V. Lyamin, M. Hjiaj, S.W. Sloan, "A new discontinuous upper bound limit analysis formulation", Int. J. Numer. Methods Eng. 63, 1069–1088, 2005.

[20] G. Maier, A. Nappi, "A theory of no-tension discretized structural systems", Eng. Struct. 12, 227–234, 1990.

[21] M.C. Ferris, F. Tin-Loi, "Limit analysis of frictional block assemblies as a mathematical program with complementarity constraints", Int. J. Mech. Sci. 43, 209–224, 2001.

[22] Y. Hua, G. Milani, "Rigid Block Limit Analysis of Masonry Arches with Associated and Non-associated Slides", in: From Corbel Arches to Double Curvature Vaults Anal. Conserv. Restor. Archit. Herit. Mason. Struct. pp. 169–203, 2022.

[23] Ministry of Housing and Urban-Rural Development of the People's Republic of China, "GB50003-2011 Code for Design of Masonry Structures", 2011. [In Chinese].

[24] G. Milani, "Fast Vulnerability Evaluation of Masonry Towers by Means of an Interactive and Adaptive 3D Kinematic Limit Analysis with Pre-assigned Failure Mechanisms", Int. J. Archit. Herit. 13, 941–962, 2019.